This is an open access article published under an ACS AuthorChoice License, which permits copying and redistribution of the article or any adaptations for non-commercial purposes.

ACS OMEGA

http://pubs.acs.org/journal/acsodf

Article

Pyridyl CO_2 Fixation Enabled by a Secondary Hydrogen Bonding Coordination Sphere

Jacqueline N. Gayton, Qing Li, Lakeeta Sanders, Roberta R. Rodrigues, Glake Hill, and Jared H. Delcamp*

Cite This: *ACS Omega* 2020, 5, 11687−11694

Read Online

ACCESS | Metrics & More | Article Recommendations | Supporting Information

ABSTRACT: Reversible CO_2 binders under ambient conditions are of significant interest for multiple applications in sensing and capture technologies. In this paper, a general systematic way to evaluate CO_2 receptors with π-systems is put forward. A series of receptors (five pyridine-based and one triazine-based) are evaluated as CO_2 binders in terms of number of hydrogen bonding sites, strength of hydrogen bond donors, and number of nucleophilic sites. The binding of CO_2 to the receptors was probed by computational models, absorption spectroscopy, fluorescence spectroscopy, cyclic voltammetry, and ^{1}H NMR studies. Multiple solvents with varying ionic strength additives are probed to analyze the effects on CO_2-bound intermediates. The receptors were screened progressively down-selecting through the different analytical techniques arriving at a promising pyridine receptor, which shows evidence of CO_2 binding with each of the analytical techniques. The diaminopyridine motif demonstrates reversible CO_2 binding and has convenient substitution sites for derivatization to incorporate into functional sensor systems.

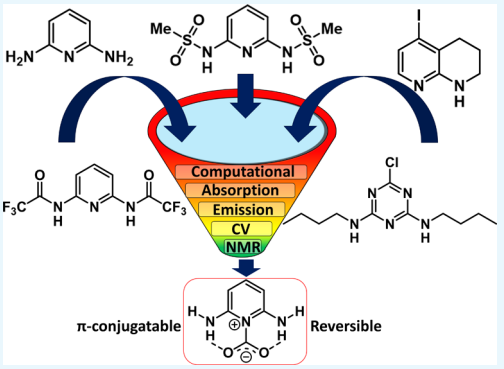

INTRODUCTION

CO_2 sensors with good sensitivity and stability are in high demand.[1−3] Additionally, CO_2 capture approaches have been a long-standing area of research interest.[4−8] Recently, a number of organic-based receptors with nucleophilic coordination sites have been studied at a fundamental level (Figure 1).

This strategy holds the potential to rapidly identify suitable functionality, which can be incorporated into reusable sensors based on organic electronics and CO_2 fixation approaches.[9−11] Present strategies predominantly work through coordination of the carbon atom of CO_2 to a nucleophilic receptor site based on an amidine nitrogen (e.g., 1,8-diazabicyclo(5.4.0)undec-7-ene, DBU),[12−14] N-heterocyclic carbene carbons,[15−18] or phosphines (Figure 1).[19] These receptors often: (1) bind CO_2 strongly, leading to incompatibility with reusable technologies without harsh conditions or chemical reactions to reverse binding (with some notable exceptions),[15,20,21] (2) are not stable under ambient conditions, and (3) are difficult to incorporate as a conjugated component in π-conjugated systems for use in organic electronics because of the lack of substitutable receptor π-system positions. Aminocarboxamidines have been shown to incorporate hydrogen bonding to an oxygen of CO_2 in addition to a nitrogen−carbon interaction, resulting in a stabilized CO_2 adduct (Figure 1).[22,23] Inspired by the recent work with pyridine-based MOF-binding CO_2,[24] we reasoned that the nucleophilicity of the Lewis basic nitrogen could be reduced by incorporation of this nitrogen into an aromatic pyridine system, which weakens electron density donation into the imine bond by substituents on the pyridine ring, allowing for reversible CO_2 binding because this donation requires loss of aromaticity in the case of substituted pyridines. To enable CO_2 bonding of significant strength, H-bonding groups of varying H-bond donor strength can be added near the nucleophilic nitrogen site. This allows for a tunable approach to strengthen or weaken CO_2 adduct formation. Additionally, aromatic systems as receptors are characterizable with optical spectroscopic techniques and electrochemical techniques more readily than aliphatic binders because of the more easily accessed π and π^* orbitals. This expands the detection methods for the receptor beyond typically used nuclear magnetic resonance (NMR) spectroscopy. This paper puts forward a general strategy for the systematic evaluation of CO_2 receptors with π-systems through an initial set of rapid analysis techniques using absorption spectroscopy, emission spectroscopy, and computational analysis. Techniques that are either more limited in environment (electrochemistry, which requires a high salt concentration) or lengthier in data

Received: March 5, 2020
Accepted: April 24, 2020
Published: May 11, 2020

ACS Publications

© 2020 American Chemical Society

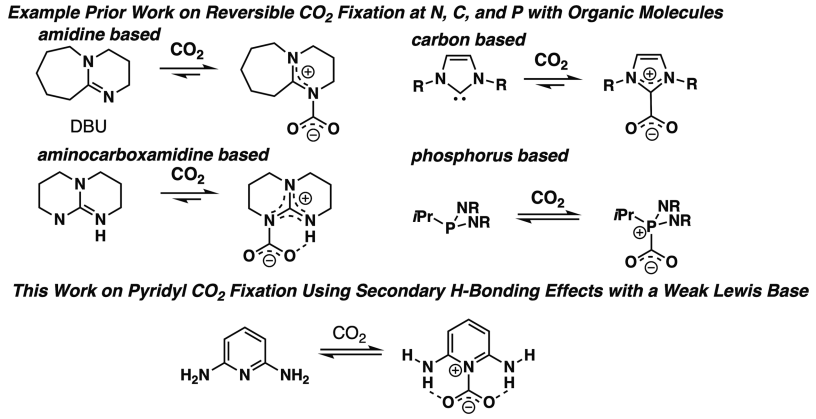

Figure 1. Example of prior CO_2 fixation strategies using strong Lewis bases (DBU,[12] NHC,[15] phosphinine,[19] and aminocarboxamidine[22]) and an example of an aromatic pyridyl CO_2 binder with hydrogen bond (H-bond) donors studied in this work.

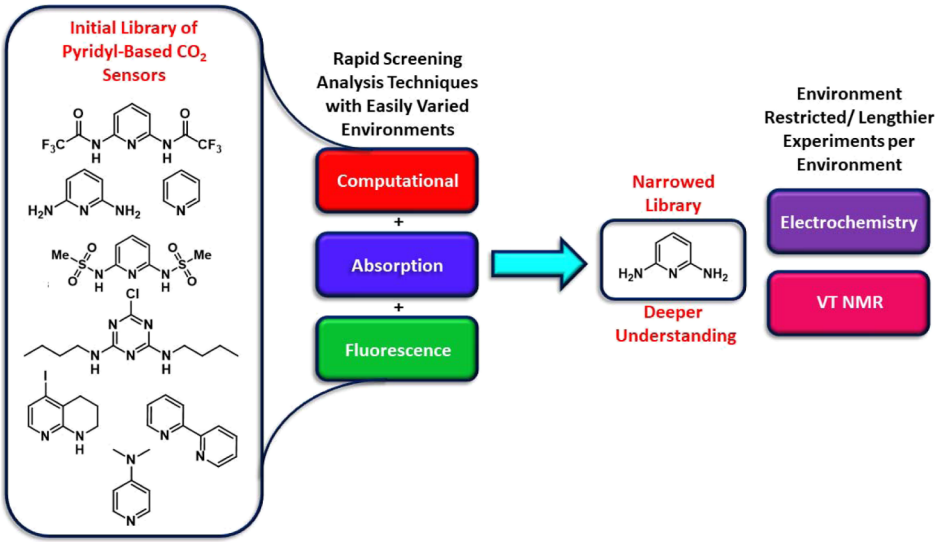

Figure 2. Down-selection of pyridyl-based receptors, according to the analysis method for CO_2 detection.

collection time (variable low-temperature ^{1}H NMR analysis) are then used to gather more data on intriguing receptors found during initial rapid screening. This general evaluation sequence allows for the rapid evaluation of eight potential CO_2 receptors by down-selecting, in which potential receptors are carried forward to the next analytical technique set (Figure 2). A down-selection approach allows quick determination of which receptors will be most suitable for use in applications for the detection of CO_2.

RESULTS AND DISCUSSION

With the goal of rapidly identifying an aromatic CO_2 receptor for incorporation into π-conjugated systems, eight initial targets were examined with varying aromatic nitrogen donor group strengths and varying H-bond donor strengths (Figure 2). The initial analysis set utilizes optical spectroscopy, which requires significant differentiation of the receptor absorption features and the solvent. Based on this criteria, pyridine, 2,2′-bipyridine, and 4-dimethylaminopyridine were excluded because of significant absorption spectrum overlap with the solvents used in this study, which have considerable CO_2 solubility. The remaining five CO_2 binding groups have both a primary pyridyl-*N* coordination to the carbon of CO_2 and a secondary hydrogen-bonding coordination sphere (Figure 3).

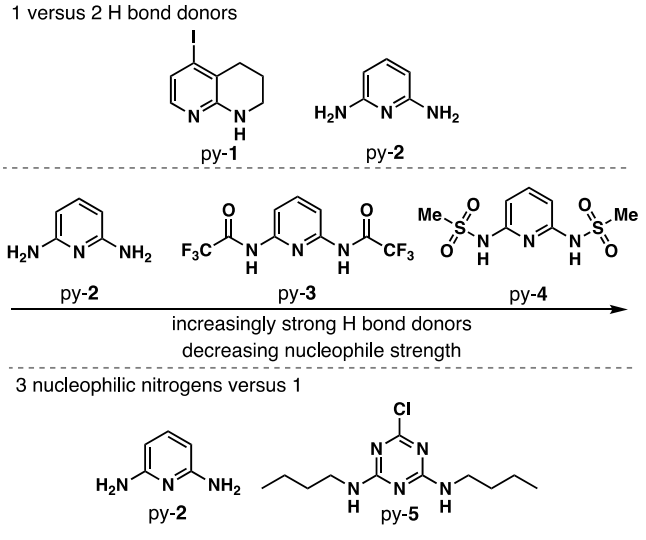

Figure 3. Target pyridine-based receptors.

The effects of one versus two hydrogen bond donors are probed by comparing 5-iodo-1,2,3,4-tetrahydro-1,8-naphthyridine (py-**1**)[25] and pyridine-2,6-diamine (py-**2**).[26] H-bond donor strength is examined by varying the substituents on the

https://dx.doi.org/10.1021/acsomega.0c00989
ACS Omega 2020, 5, 11687−11694

Table 1. Selected Computational Data for the Receptors in the Presence and Absence of CO_2

Receptor	HOMO (eV)	LUMO (eV)	orbitals ($S_0 \rightarrow S_1$)	% Cont.	vert. trans (nm|eV)	Osc. strength	dipole (D)	N−C bond length (Å)	H−O bond length (Å)
py-1	−7.132	0.080	H → L	67%	264|4.70	0.045	2.23		
			H → L + 1	29%					
py-1-CO_2	−7.167	0.020	H → L	48%	266|4.65	0.079	2.29	2.68	2.25
			H → L + 1	47%					
py-1 Δ + CO_2	−35 mV	−40 mV		↑H → L + 1	+2 nm	+0.034	+0.06		
py-2	−6.683	0.920	H → L	92%	252|4.92	0.133	0.26		
			H-1 → L + 1	5%					
py-2-CO_2	−6.669	0.839	H → L	93%	256|4.85	0.133	0.52	2.83	2.17
			H-1 → L + 1	4%					
py-2 Δ + CO_2	+14 mV	−81 mV			+4 nm		+0.26		
py-3	−8.415	−0.808	H → L	89%	247|5.01	0.281	0.81		
			H-1 → L + 1	4%					
			H-5 → L + 1	3%					
py-3-CO_2	−8.377	−0.844	H → L	90%	251|4.95	0.282	1.19	2.94	2.07
			H-1 → L + 1	3%					
			H-5 → L + 1	3%					
py-3 Δ + CO_2	+38 mV	−36 mV			+4 nm	+0.001	+0.38		
py-4	−8.207	−0.442	H → L	91%	246|5.05	0.203	6.17		
			H-1 → L + 1	6%					
py-4-CO_2	−8.237	−0.575	H → L	92%	249|4.97	0.203	6.02	2.81	2.42
			H-1 → L + 1	5%					
py-4 Δ + CO_2	−30 mV	−133 mV			+3 nm		−0.15		
py-5	−8.098	0.439	H-1 → L	86%	221|5.60	0.095	4.19		
			H → L + 1	10%					
py-5-CO_2	−8.136	0.351	H → L	88%	223|5.55	0.116	4.04	2.78	2.18
			H-1 → L + 1	7%					
py-5 Δ + CO_2	−38 mV	−88 mV			+2 nm	+0.021	−0.15		

H-bond donor nitrogen atoms with H on py-**2**, trifluoroacetyl groups on py-**3**,[27] and methanesulfonyl groups on py-**4**.[28] This provides a range of electron-withdrawing substituent strengths on the H-bond donor nitrogen atoms, resulting in a range of acidities, which modulates H-bond donor strength. The number of nucleophilic nitrogens is compared between one (py-**2**) and three with triazine-derivative py-**5**.[29] As an illustration of how these receptors could be incorporated into π-functional systems, halide functional handles are present on py-**1** and py-**5**.[25] This collection of receptors offers a range of both nucleophilicity and hydrogen bonding strengths, and each receptor is easily obtained from known synthetic routes in literature with py-**2** being commercial.[25−27,29]

Computational studies were undertaken to assess the viability of each CO_2 receptor for binding based on electronic properties and coordination geometry at the M06-2X[30]/6-311G(d) level with the Gaussian 16 software package using density functional theory (DFT).[31] The receptors all show reasonable bond lengths for binding of both the N atom of the receptor to the C atom of CO_2 and the H atom of the receptor to the O atoms of CO_2 with bond lengths ranging from 2.68 to −2.94 and 2.07 to 2.42 Å, respectively. CO_2 binds in a coplanar geometry relative to the aromatic ring with the exception of py-**4**, which shows the CO_2 binding above the plane of the aromatic ring. The highest occupied molecular orbital (HOMO) and lowest unoccupied molecular orbital (LUMO) energies were evaluated along with the vertical transitions and oscillator strengths for each receptor both in the presence and absence of CO_2 (Table 1). A change in orbital energies is expected upon addition of CO_2 as an electron-accepting group near the aromatic nitrogen group. This would be expected to lower the LUMO energy primarily based on first principles analysis. Notably, the LUMO position remains on the aromatic group and consistently decreases in energy for each receptor in the presence of CO_2 (Table 1, Figure S23). The observed trend for the difference between the LUMO energy values for receptors with and without CO_2 is py-**4** > py-**5** > py-**2** > py-**1** > py-**3**. Py-**4** has the largest change in LUMO energy, which is also correlated with py-**4** having the strongest H-bond donating strength because of the strongly withdrawn sulfonyl groups. However, no obvious trend emerges from this series based on number of H-bond donors, nucleophilic nitrogen strength, or H-bond donor strength. The HOMO orbital energies shift by only modest amounts both toward higher and lower energy upon coordination of CO_2. The molecular dipole would be expected to strengthen upon CO_2 binding if the molecule dipole is oriented toward the nitrogen binding group in the aryl ring because CO_2 is an acceptor that would further polarize the molecule. This is the case for py-**1**, py-**2**, and py-**3**. However, for py-**4** and py-**5**, the dipole is not oriented toward the nitrogen binding group, and the dipole is found to weaken upon coordination of CO_2. Among the receptors with the dipole oriented toward CO_2, which could lead to stronger binding, py-**2** has the largest change in LUMO energy, suggesting that this receptor could be intriguing for future studies.

https://dx.doi.org/10.1021/acsomega.0c00989
ACS Omega 2020, 5, 11687−11694

Electronic transitions were analyzed by time-dependent (TD)-DFT at the same level of theory used for the geometry optimizations. Percent contributions of the orbitals to the S0 → S1 transition are comparable for all receptors and are primarily HOMO to LUMO transitions with the exception of py-**1**, which has a relatively higher contribution from the H → L + 1 orbital of 29 and 47% in the absence and presence of CO_2, respectively. The vertical transitions range from 221 to 264 nm with an observed shift of 2−4 nm in the presence of CO_2 for each receptor. This shift is expected because the addition of an electron-accepting CO_2 group to the nitrogen donor should lower the LUMO energy and decrease the optical gap. Overall, the computational results suggest that CO_2 binding can occur with these receptors, and optical changes may be observable via absorption and emission spectroscopy.

A series of photophysical studies via absorption and fluorescence spectroscopy in three solvents [dimethylformamide (DMF), tetrahydrofuran (THF), and acetonitrile (MeCN)] were performed. The solvents were selected based on varying dipoles (1.75−3.92 D), varying dielectric constants (8−38), and good CO_2 solubility (0.20−0.28 M).[32] Additionally, tetrabutylammonium hexafluorophosphate ($TBAPF_6$) was added to the solutions to probe the effects of increasing the dielectric constant on CO_2 binding because bound intermediates may have localized charge on the nitrogen donor atom or the oxygen atoms of CO_2.[12,33] Additionally, the dipole was found to strengthen upon coordination of CO_2 in several cases computationally, and the addition of a salt to the solution may aid in stabilizing the molecular dipole upon CO_2 coordination. Experiments were conducted by performing initial measurements under nitrogen, followed by measurements in a saturated solution of CO_2 under a CO_2 atmosphere. The receptors were measured in each solvent where the receptor had appreciable solubility with minimal spectral overlap with the solvent. Py-**2** uniquely shows a significant response via absorption spectroscopy in THF (Figure 4). A

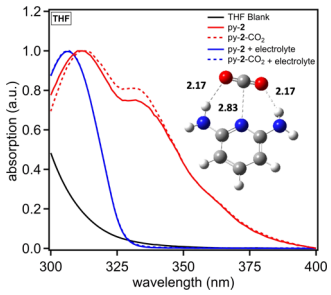

Figure 4. Absorption spectrum of py-**2** in THF with and without $TBAPF_6$ electrolyte. An image of a CO_2 bound to py-**2** with labeled bond distances is overlaid.

shoulder at ∼335 nm shows a non-negligible increase in absorption intensity under CO_2 relative to N_2, which is strong evidence of py-**2**-binding CO_2 in the ground state. The introduction of CO_2 to the solution resulted in an increase of 6% absorption intensity induced by the binding of CO_2, leading to a stronger optical transition. The reason for this increase in absorption strength was not apparent from these studies. Structurally, py-**2** represents an extreme in the series being probed with the strongest nitrogen nucleophile because of the two strong ortho amine donor atoms. Py-**2** also has the weakest H-bond donors. Interestingly, seemingly both H-bond donors via two amine activating groups need to be present to observe a binding effect because py-**1** with one hydrogen bonding amine group shows no evidence of CO_2 binding via absorption spectroscopy. The remaining receptors show no dramatic changes in the absorption spectrum (Figures S1−S11).

Computational studies at the M06-2X[30]/6-311G(d) level with the Gaussian 16 software package[31] show a preferred binding geometry with both amine groups on py-**2** hydrogen bonding at a distance of 2.17 Å with the nucleophilic nitrogen binding the carbon of CO_2 at a distance of 2.83 Å (Figure 4). Notably, the structure slightly desymmetrizes with one of the amine groups rotating the hydrogen further out of the aryl plane. No significant change in the frontier molecular orbital positions is observed (Figure S23). TD-DFT at the M06-2X/6-311G(d) level predicts a slight red shift of the absorption spectrum by about 4 nm when CO_2 is bound. This is consistent with the small shift (∼1 nm) in the absorption curve for the higher energy peak at 312 nm when CO_2 is added.

Fluorescence spectroscopy was probed next for each receptor in each solvent with and without $TBAPF_6$ being added. In general, fluorescence is an exceptionally sensitive optical measurement technique, allowing for subtle changes to the fluorophore environment to result in significant signal changes. Significant shifts are noted for all of the receptors when emission curves under N_2 and CO_2 are compared for at least one solvent (Figures 5 and S12−S18). The solvents with the most dramatic shifts in curve shapes and emission energies are shown in Figure 5 with the remaining curves in the Supporting Information. In DMF, py-**1** shows a relative increase in emission intensity in the 370−390 nm wavelength region when the other regions are normalized. Only one of the emission band features increases in intensity, which could be due a new species in solution because of CO_2 binding. When $TBAPF_6$ is added, the effect remains, although it is present to a lesser extent. The most dramatic change in the emission curve signals occurs when CO_2 and N_2 are compared with py-**2** in the presence of $TBAPF_6$ in THF. Under N_2, the emission curve has three features. The two most intense curve features under N_2 diminish dramatically when CO_2 is added with a dominate high energy peak remaining. This large shift in emission intensity (∼40% lower with CO_2) and wavelength (∼50 nm) suggests significant interactions with CO_2 when the solution dielectric constant is increased by addition of $TBAPF_6$. This may indicate that the electrolyte is promoting the formation of a zwitter ionic-like py-**2**-CO_2 adduct.[12] Py-**3** and py-**4** uniquely show increases in emission intensity in the lower energy region of the spectrum with and without electrolyte in acetonitrile. The remaining receptors show either loss of low-energy emission intensity or an increase in high-energy emission intensity. Py-**3** and py-**4** are unique among the receptors in which they have the strongest hydrogen bond-donating groups and weakest nitrogen nucleophile. This combination is correlated via these studies to an increase in low-energy emission intensity. Py-**5** shows a significant change in the emission curve shape in DMF only when $TBAPF_6$ is present with a response similar to that observed for py-**1**.

Among the receptors, py-**2** shows the only significant response via absorption spectroscopy and the most dramatic response via fluorescence spectroscopy. Py-**2** was exclusively used in the next set of analytical techniques [cyclic voltammetry (CV) and NMR] after rapid computational and

https://dx.doi.org/10.1021/acsomega.0c00989
ACS Omega 2020, 5, 11687−11694

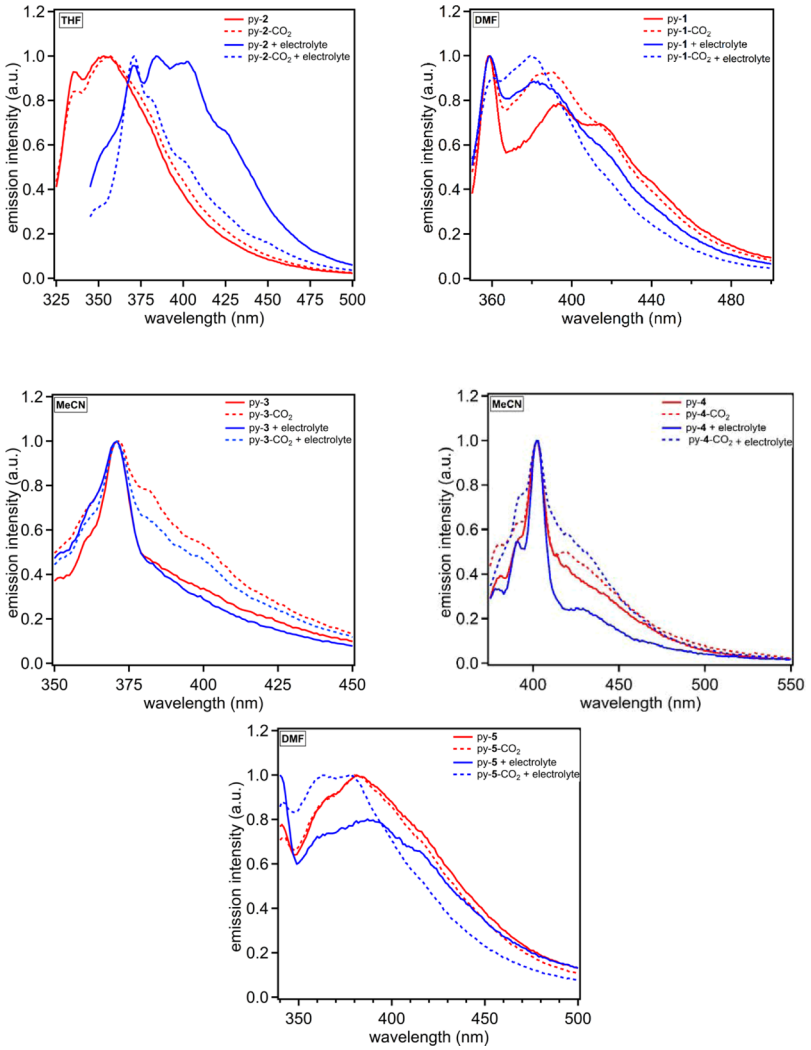

Figure 5. Emission spectra of py-**1** in DMF (top left), py-**2** in THF (top right), py-**3** in MeCN (middle left), py-**4** in MeCN (middle right), and py-**5** in DMF (bottom). The solid lines denote under an inert atmosphere, and dashed lines represent the presence of CO_2. Red curves are in the absence of $TBAPF_6$, and blue curves are in the presence of 0.1 M $TBAPF_6$.

optical property screening show this receptor to be the most promising (Figure 2). Based on this data, a strong nitrogen nucleophile may be the dominate effect, governing interactions with CO_2, with the hydrogen bonding groups serving as a secondary role. Py-**2** was then used for additional electrochemical and NMR studies. Signal responses are expected for both techniques because this receptor shows strong binding properties in THF via optical measurements. Upon binding of the nucleophilic nitrogen to CO_2, a loss of electron density on the pyridine ring is expected because of the buildup of a partial positive charge on the nitrogen atom. A loss of electron density would be expected to present as a shift in electrochemical peak oxidation potentials toward more positive values whereas the receptor would become more difficult to oxidize. Thus, CV studies were undertaken with py-**2** in THF to probe if CO_2 is associated in this solution (Figure 6, see Figure S19 for a wider scan window). Under argon, two oxidation waves are observed with weak, pseudo reversibility with peak potentials of 0.51 and 1.13 V versus ferrocenium/ferrocene (Fc^+/Fc). Upon addition of CO_2, these peaks shift as hypothesized to more positive oxidation potentials by 0.04 and 0.07 V, which is indicative of an electron-withdrawing moiety such as CO_2 being added to the compound. This shift in potential is indicative of a receptor

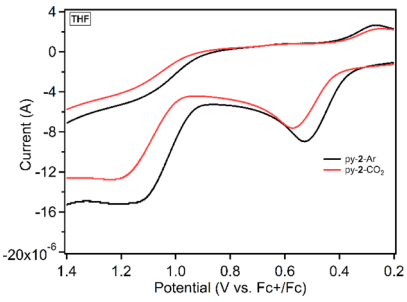

Figure 6. Cyclic voltammogram of 4 mM py-**2** in THF with 0.1 M $TBAPF_6$ under argon and CO_2.

binding CO_2 in the ground state as is commonly observed for electrocatalytic CO_2 reduction reactions.[34] Notably, the reduction potential of the receptor is outside the electrochemical solvent/electrolyte window.

Variable temperature (VT) ^{1}H NMR studies were undertaken with py-**2** in THF-d_8 under N_2 and with CO_2 to analyze binding event equilibrium temperatures and to better characterize the CO_2-bound py-**2** species (Figure 7, see Figures S20−S22 for the spectrum in CD_3CN and DMF-d_7).

https://dx.doi.org/10.1021/acsomega.0c00989
ACS Omega 2020, 5, 11687−11694

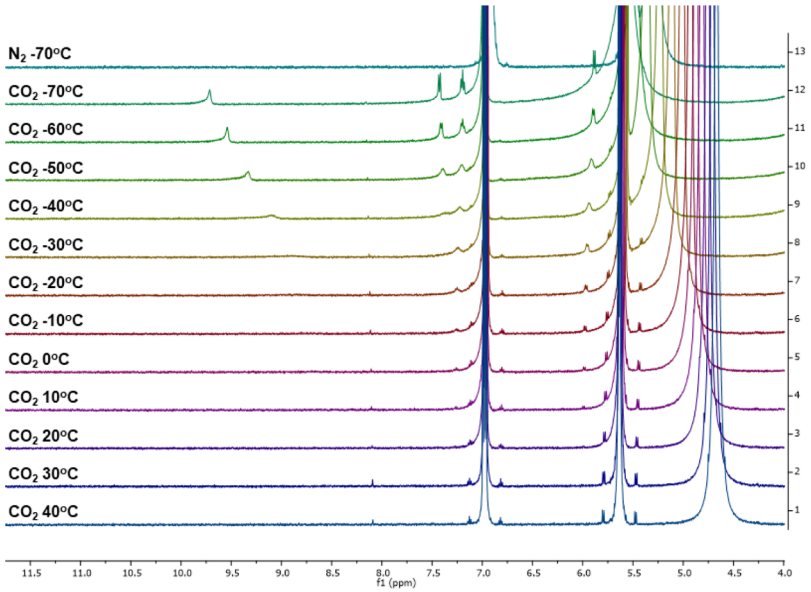

Figure 7. ^{1}H NMR data showing CO_2 binding with py-**2** in THF-d_8.

In THF-d_8, the free py-**2** is observed primarily in solution in the presence of CO_2. However, beginning at 10 °C, small amounts of a new species can be observed at 5.97 and 7.24 ppm near the satellite peaks for the free py-**2**. The new species continues to grow as colder temperatures are reached to the experimental limit of our setup at −70 °C. At −70 °C, four well resolved peaks can be identified in the spectrum as two doublets (5.89 and 7.42 ppm) and a triplet (7.19 ppm) at similar estimated integrations. These signals are assigned to the aromatic protons on the py-**2** receptor. Additionally, a peak shifting significantly with temperature is observed from −30 °C (9.08 ppm) to −70 °C (9.71 ppm). This peak is attributed to one of the N−H bonds on py-**2** with the other signal not being observed. These data suggest that the CO_2-bound py-**2** complex is not symmetric (as suggested by DFT) because of a differentiation in all of the aromatic signals and estimated integration giving equal hydrogen counts. Importantly, at −70 °C under N_2, no new signals are observed, which suggests that the new signals under CO_2 are because of formation of a py-**2**-CO_2 adduct. Similar behavior is observed for py-**2** in CD_3CN (Figure S20) and DMF-d_7 (Figure S21) via VT ^{1}H NMR, although the temperature range was limited due to the higher melting points of these solvents relative to THF-d_8. CD_3CN shows the presence of peaks assigned to the CO_2-bound py-**2**, appearing clearly at −20 °C, which is about 30 °C lower in temperature than was required to see the peaks in THF-d_8. DMF-d_7 shows new peaks first appearing at about 0 °C, which is near the same temperature as they appear in THF-d_8. It is consistent that the interaction of py-**2** with CO_2 could be observed at the highest temperatures in THF, and that the optical data obtained for py-**2** with CO_2 at room temperature gave the most dramatic evidence of binding among the receptors. At the lowest temperature measured with DMF-d_8, strong signals are observed for the new species with the most down-field signal being observed at 16 ppm. A shift, this far, down-field is diagnostics of strongly hydrogen-bonded proton signals or acidic hydrogens, which could occur upon CO_2 binding to py-**2**.[35] Notably, all of the signals attributed to a py-**2**-CO_2 adduct disappear at room temperature, which indicates that py-**2** is serving as a reversible CO_2 binder.

CONCLUSIONS

In conclusion, a series of pyridine-based receptors were evaluated for binding of CO_2. Increasing the number of hydrogen binding sites on strongly donating atoms from one to two dramatically increased the binding of CO_2. Stronger hydrogen bond donors were found to decrease CO_2 binding strength, suggesting that this is weaker secondary effect relative to the primary effect of a nucleophilic nitrogen binding. This finding highlights the importance of the nucleophilic site in contrast with the hydrogen bonding site. The 2,6-diaminopyridine receptor was shown to bind CO_2 by absorption spectroscopy, fluorescence spectroscopy, CV studies, and ^{1}H NMR studies. The NMR studies show a reversible system, highlighting the applicability of these receptors to technologies for CO_2 fixation and reversible sensors. Readily available functional handles on the receptors enable their use in a variety of applications such as OFET sensors, which is being pursued as a future direction.

EXPERIMENTAL SECTION

Spectroscopic-grade MeCN and DMF were used as received from the supplies. THF was passed through a solvent transfer system using a bed of alumina as a drying reagent and was kept under argon. *Absorption spectroscopy* data were collected on a Cary 5000 UV−vis−NIR spectrometer. The receptor (1 mg, 1.2 mM) was dissolved in 10 mL of solvent with 0.1 M $TBAPF_6$ present when noted. A blank of the same solvent that was used to prepare the solutions was used to serve as the background during absorption spectroscopy data acquisition. The solution (3 mL) was pipetted into a clean, dry, and sealable cuvette. The solvent level was marked, and then 0.15 mL of pure solvent was added. The sample was then degassed with nitrogen until the solvent level returned to the original marked level before data were acquired. This procedure was replicated for CO_2. *Fluorescence data* were collected on a Horiba FluoroMax SpectroFluorimeter. Samples were prepared identically as described for the absorption spectroscopy studies. Each receptor was photoexcited at the maximum absorption peak for the lowest energy transition from the absorption curve. Computational data were collected using the

https://dx.doi.org/10.1021/acsomega.0c00989
ACS Omega 2020, 5, 11687−11694

M06-2X[30]/6-311G(d) level with the Gaussian 16 software package.[31]

Cyclic Voltammetry data were collected on a CH Instruments Electrochemical Analyzer (CHI602E). A 0.1 M solution of tetrabutylammonium hexafluorophosphate was used as the electrolyte with THF as the solvent. A glassy carbon working electrode, platinum counter electrode, and silver wire reference electrode were submerged in the electrolyte solution within a sealable three-necked flask. The system was then degassed with argon until the solvent level returns to the original level after addition of 0.2 mL of pure solvent. py-**2** (1.3 mg, 4 mM) is added into the flask along with 0.2 mL of pure solvent. The solution is once again degassed with argon until the original solvent level is reached before data acquisition. The same procedure is repeated with CO_2 in place of argon. Ferrocene was used as an internal reference in the CV studies.

NMR experiments were performed with Avance 500 MHz NMR. Samples were prepared by dissolving 3 mg of 2,6-diaminopyridine in THF-d_8, CD_3CN, or DMF-d_7. Nitrogen was bubbled through each NMR tube for 30 s, followed by carbon dioxide bubbling for 30 s, and then the tube was sealed with a screw cap for NMR analysis. Variable temperature was performed beginning at low temperature and ramping up in 10° increments. Each spectrum was referenced to the deuterated solvent peak using IconNMR software.

■ ASSOCIATED CONTENT

Supporting Information

The Supporting Information is available free of charge at https://pubs.acs.org/doi/10.1021/acsomega.0c00989.

Full cyclic voltammogram of py-**2** and ^{1}H characterization of py-**2** in MeCN-d_3, DMF-d_7, and THF-d_8 along with computational data (PDF)

■ AUTHOR INFORMATION

Corresponding Author

Jared H. Delcamp − *Department of Chemistry and Biochemistry, University of Mississippi, University, Mississippi 38677, United States;* orcid.org/0000-0001-5313-4078; Email: delcamp@olemiss.edu

Authors

Jacqueline N. Gayton − *Department of Chemistry and Biochemistry, University of Mississippi, University, Mississippi 38677, United States;* orcid.org/0000-0002-3564-1663

Qing Li − *Department of Chemistry and Biochemistry, University of Mississippi, University, Mississippi 38677, United States*

Lakeeta Sanders − *Department of Chemistry, Jackson State University, Jackson, Mississippi 39217, United States*

Roberta R. Rodrigues − *Department of Chemistry and Biochemistry, University of Mississippi, University, Mississippi 38677, United States;* orcid.org/0000-0003-2930-2451

Glake Hill − *Department of Chemistry, Jackson State University, Jackson, Mississippi 39217, United States*

Complete contact information is available at: https://pubs.acs.org/10.1021/acsomega.0c00989

Author Contributions

The manuscript was written through contributions of all the authors. All the authors have given approval to the final version of the manuscript. Compounds were synthesized by J.N.G, R.R.R., and J.H.D. Photophysical properties were measured by Q.L. and J.H.D. Proton spectra were collected by J.N.G. Computational data were collected by L.S. and G.H.

Funding

This work was supported by NSF OIA-1632825.

Notes

The authors declare no competing financial interest.

■ ACKNOWLEDGMENTS

The authors thank NSF for award OIA-1632825, which supported all of these studies. Q.L. thanks the Sally McDonnell Barksdale Honors College for supporting this work toward her thesis. The University of Alabama NMR facilities are thanked for assistance with the variable temperature studies.

■ REFERENCES

(1) Chatterjee, C.; Sen, A. Sensitive Colorimetric Sensors for Visual Detection of Carbon Dioxide and Sulfur Dioxide. *J. Mater. Chem. A* **2015**, *3*, 5642−5647.

(2) Zhou, X.; Lee, S.; Xu, Z.; Yoon, J. Recent Progress on the Development of Chemosensors for Gases. *Chem. Rev.* **2015**, *115*, 7944−8000.

(3) Bowman-James, K.; Bianchi, A.; Garcia-Espana, E. *Anion Coordination Chemistry*; Wiley Anion Coordination Chemistry, 2012.

(4) Darabi, A.; Jessop, P. G.; Cunningham, M. F. CO_2-Responsive Polymeric Materials: Synthesis, Self-Assembly, and Functional Applications. *Chem. Soc. Rev.* **2016**, *45*, 4391−4436.

(5) Islamoglu, T.; Behera, S.; Kahveci, Z.; Tessema, T. D.; Jena, P.; El-Kaderi, H. M. Enhanced Carbon Dioxide Capture from Landfill Gas Using Bifunctionalized Benzimidazole-Linked Polymers. *ACS Appl. Mater. Interfaces* **2016**, *8*, 14648.

(6) Sanz-Pérez, E. S.; Murdock, C. R.; Didas, S. A.; Jones, C. W. Direct Capture of CO_2 from Ambient Air. *Chem. Rev.* **2016**, *116*, 11840.

(7) Rochelle, G. T. Amine Scrubbing for CO_2 Capture. *Science* **2009**, *325*, 1652−1654.

(8) Keith, D. W. Why Capture CO_2 from the Atmosphere. *Science* **2009**, *325*, 1654−1655.

(9) Torsi, L.; Magliulo, M.; Manoli, K.; Palazzo, G. Organic Field-Effect Transistor Sensors: A Tutorial Review. *Chem. Soc. Rev.* **2013**, *42*, 8612−8628.

(10) Lee, Y. H.; Jang, M.; Lee, M. Y.; Kweon, O. Y.; Oh, J. H. Flexible Field-Effect Transistor-Type Sensors Based on Conjugated Molecules. *Chem* **2017**, *3*, 724−763.

(11) Li, H.; Shi, W.; Song, J.; Jang, H.-J.; Dailey, J.; Yu, J.; Katz, H. E. Chemical and Biomolecule Sensing with Organic Field-Effect Transistors. *Chem. Rev.* **2019**, *119*, 3−35.

(12) Heldebrant, D. J.; Jessop, P. G.; Thomas, C. A.; Eckert, C. A.; Liotta, C. L. The Reaction of 1,8-Diazabicyclo[5.4.0]undec-7-ene (DBU) with Carbon Dioxide. *J. Org. Chem.* **2005**, *70*, 5335−5338.

(13) Pereira, F. S.; Lincon da Silva Agostini, D.; do Espírito Santo, R. D.; deAzevedo, E. R.; Bonagamba, T. J.; Job, A. E.; González, E. R. P. A Comparative Solid State 13C NMR and Thermal Study of CO_2 Capture by Amidines PMDBD and DBN. *Green Chem.* **2011**, *13*, 2146.

(14) Mercy, M.; Rebecca Taylor, S. F.; Jacquemin, J.; Hardacre, C.; Bell, R. G.; De Leeuw, N. H. The Addition of CO_2 to Four Superbase Ionic Liquids: A DFT Study. *Phys. Chem. Chem. Phys.* **2015**, *17*, 28674−28682.

(15) Van Ausdall, B. R.; Glass, J. L.; Wiggins, K. M.; Aarif, A. M.; Louie, J. A Systematic Investigation of Factors Influencing the Decarboxylation of Imidazolium Carboxylates. *J. Org. Chem.* **2009**, *74*, 7935−7942.

(16) Kayaki, Y.; Yamamoto, M.; Ikariya, T. N-Heterocyclic Carbenes as Efficient Organocatalysts for CO_2 Fixation Reactions. *Angew. Chem., Int. Ed.* **2009**, *48*, 4194−4197.

(17) Riduan, S. N.; Zhang, Y.; Ying, J. Y. Conversion of Carbon Dioxide into Methanol with Silanes over N-Heterocyclic Carbene Catalysts. *Angew. Chem., Int. Ed.* **2009**, *48*, 3322−3325.
(18) Yang, L.; Wang, H. Recent Advances in Carbon Dioxide Capture, Fixation, and Activation by Using N-Heterocyclic Carbenes. *ChemSusChem* **2014**, *7*, 962−998.
(19) Buss, F.; Mehlmann, P.; Mück-Lichtenfeld, C.; Bergander, K.; Dielmann, F. Reversible Carbon Dioxide Binding by Simple Lewis Base Adducts with Electron-Rich Phosphines. *J. Am. Chem. Soc.* **2016**, *138*, 1840−3.
(20) Pinaud, J.; Vignolle, J.; Gnanou, Y.; Taton, D. Poly(N-Heterocyclic-Carbene)s and Their CO_2 Adducts as Recyclable Polymer-Supported Organocatalysts for Benzoin Condensation and Transesterification Reactions. *Macromolecules* **2011**, *44*, 1900−1908.
(21) Fèvre, M.; Pinaud, J.; Gnanou, Y.; Vignolle, J.; Taton, D. N-Heterocyclic Carbenes (NHCs) as Organocatalysts and Structural Components in Metal-Free Polymer Synthesis. *Chem. Soc. Rev.* **2013**, *42*, 2142−2172.
(22) Villiers, C.; Dognon, J.-P.; Pollet, R.; Thuéry, P.; Ephritikhine, M. An Isolated CO_2 Adduct of a Nitrogen Base: Crystal and Electronic Structures. *Angew. Chem., Int. Ed.* **2010**, *49*, 3465−3468.
(23) Das Neves Gomes, C.; Jacquet, O.; Villiers, C.; Thuery, P.; Ephritikhine, M.; Cantat, T. A Diagonal Approach to Chemical Recycling of Carbon Dioxide: Organocatalytic Transformation for the Reductive Functionalization of CO_2. *Angew. Chem., Int. Ed.* **2012**, *51*, 187−190.
(24) Deria, P.; Li, S.; Zhang, H.; Snurr, R. Q.; Hupp, J. T.; Farha, O. K. A Mof Platform for Incorporation of Complementary Organic Motifs for CO_2 Binding. *Chem. Commun.* **2015**, *51*, 12478−12481.
(25) Nguyen, H. N.; Wang, Z. J. Novel Preparation of Functionalized Iodotetrahydronaphthyridine, Iodoazaindoline, and Iodotetrahydropyridoazepine Systems. *Tetrahedron Lett.* **2007**, *48*, 7460−7463.
(26) Elmkaddem, M. K.; Fischmeister, C.; Thomas, C. M.; Renaud, J.-L. Efficient Synthesis of Aminopyridine Derivatives by Copper Catalyzed Amination Reactions. *Chem. Commun.* **2010**, *46*, 925−927.
(27) Bolz, I.; Schaarschmidt, D.; Rüffer, T.; Lang, H.; Spange, S. A Pyridinium-Barbiturate-Betaine Dye with Pronounced Negative Solvatochromism: A New Approach for Molecular Recognition. *Angew. Chem., Int. Ed.* **2009**, *48*, 7440−7443.
(28) Ho, P. H.; Tsai, M. S.; Lee, G. H.; Che, C. M.; Peng, S. M. Novel Multinuclear Cyclic and V-shaped Cuprous Clusters with Short and Unsupported Cu(I)-Cu(I) Separations. *J. Chin. Chem. Soc.* **2013**, *60*, 813−822.
(29) Zhang, W.; Nowlan, D. T., III; Thomson, L. M.; Lackowski, W. M.; Simanek, E. E. Orthogonal, Convergent Syntheses of Dendrimers Based on Melamine with One or Two Unique Surface Sites for Manipulation. *J. Am. Chem. Soc.* **2001**, *123*, 8914−8922.
(30) Zhao, Y.; Truhlar, D. G. The M06 Suite of Density Functionals for Main Group Thermochemistry, Thermochemical Kinetics, Noncovalent Interactions, Excited States, and Transition Elements: Two New Functionals and Systematic Testing of Four M06-Class Functionals and 12 Other Functionals. *Theor. Chem. Acc.* **2008**, *120*, 215−241.
(31) Frisch, M. J.; Trucks, G. W.; Schlegel, H. B.; Scuseria, G. E.; Robb, M. A.; Cheeseman, J. R.; Scalmani, G.; Barone, V.; Petersson, G. A.; Nakatsuji, H.; Li, X.; Caricato, M.; Marenich, A. V.; Bloino, J.; Janesko, B. G.; Gomperts, R.; Mennucci, B.; Hratchian, H. P.; Ortiz, J. V.; Izmaylov, A. F.; Sonnenberg, J. L.; Williams-Young, D.; Ding, F.; Lipparini, F.; Egidi, F.; Goings, J.; Peng, B.; Petrone, A.; Henderson, T.; Ranasinghe, D.; Zakrzewski, V. G.; Gao, J.; Rega, N.; Zheng, G.; Liang, W.; Hada, M.; Ehara, M.; Toyota, K.; Fukuda, R.; Hasegawa, J.; Ishida, M.; Nakajima, T.; Honda, Y.; Kitao, O.; Nakai, H.; Vreven, T.; Throssell, K.; Montgomery, J. A., Jr.; Peralta, J. E.; Ogliaro, F.; Bearpark, M. J.; Heyd, J. J.; Brothers, E. N.; Kudin, K. N.; Staroverov, V. N.; Keith, T. A.; Kobayashi, R.; Normand, J.; Raghavachari, K.; Rendell, A. P.; Burant, J. C.; Iyengar, S. S.; Tomasi, J.; Cossi, M.; Millam, J. M.; Klene, M.; Adamo, C.; Cammi, R.; Ochterski, J. W.; Martin, R. L.; Morokuma, K.; Farkas, O.; Foresman, J. B.; Fox, D. J. *Gaussian 16*, Revision A.03; Gaussian, Inc.: Wallingford CT, 2016.
(32) Jitaru, M. Electrochemical Carbon Dioxide Reduction - Fundamental and Applied Topics. *J. Univ. Chem. Technol. Metall.* **2007**, *42*, 333−344.
(33) Goldfarb, D. L.; Corti, H. R. Electrical Conductivity of Decamethylferrocenium Hexafluorophosphate and Tetrabutylammonium Hexafluorophosphate in Supercritical Trifluoromethane. *J. Phys. Chem. B* **2004**, *108*, 3358−3367.
(34) Boudreaux, C. M.; Liyanage, N. P.; Shirley, H.; Siek, S.; Gerlach, D. L.; Qu, F.; Delcamp, J. H.; Papish, E. T. Ruthenium(II) Complexes of Pyridinol and N-Heterocyclic Carbene Derived Pincers as Robust Catalysts for Selective Carbon Dioxide Reduction. *Chem. Commun.* **2017**, *53*, 11217−11220.
(35) Bolz, I.; Moon, C.; Enkelmann, V.; Brunklaus, G.; Spange, S. Probing Molecular Recognition in the Solid-State by Use of an Enolizable Chromophoric Barbituric Acid. *J. Org. Chem.* **2008**, *73*, 4783−4793.

https://dx.doi.org/10.1021/acsomega.0c00989
ACS Omega 2020, 5, 11687−11694